LAWRENCE
LIVERMORE
NATIONAL
LABORATORY

LLNL-PROC-646620

Advances in Shock Timing Experiments on the National Ignition Facility

H. F. Robey, P. M. Celliers, J. D. Moody, J. Sater, T. Parham, B. Kozioziemski, R. Dylla-Spears, J. S. Ross, S. LePape, J. E. Ralph, M. Hohenberger, E. L. Dewald, L. Berzak-Hopkins, J. J. Kroll, B. E. Yoxall, A. V. Hamza, T. R. Boehly, A. Nikroo, O. L. Landen, M. J. Edwards

November 21, 2013

Inertial Fusion Sciences and Applications 2013
Nara, Japan
September 9, 2013 through September 13, 2013

Disclaimer

Advances in shock timing experiments on the National Ignition Facility

H F Robey[1], P M Celliers[1], J D Moody[1], J Sater[1], T Parham[1], B Kozioziemski[1], R Dylla-Spears[1], J S Ross[1], S LePape[1], J E Ralph[1], M Hohenberger[2], E L Dewald[1], L Berzak Hopkins[1], J J Kroll[1], B E Yoxall[1], A V Hamza[1], T R Boehly[2], A Nikroo[3], O L Landen[1] and M J Edwards[1]

[1]Lawrence Livermore National Laboratory, 7000 East Ave., Livermore, CA 94550 USA
[2]Laboratory for Laser Energetics, Univ. of Rochester, Rochester, New York 14623, USA
[3]General Atomics, 3550 General Atomics Court, San Diego, CA, 29186, USA

Abstract. Recent advances in shock timing experiments and analysis techniques now enable shock measurements to be performed in cryogenic deuterium-tritium (DT) ice layered capsule implosions on the National Ignition Facility (NIF). Previous measurements of shock timing in inertial confinement fusion (ICF) implosions were performed in surrogate targets, where the solid DT ice shell and central DT gas were replaced with a continuous liquid deuterium (D2) fill. These previous experiments pose two surrogacy issues: a material surrogacy due to the difference of species (D2 vs. DT) and densities of the materials used and a geometric surrogacy due to presence of an additional interface (ice/gas) previously absent in the liquid-filled targets. This report presents experimental data and a new analysis method for validating the assumptions underlying this surrogate technique.

1. Introduction

Inertial confinement capsule implosions on the National Ignition Facility (NIF) are performed using the indirect-drive concept [1], where the energy of a temporally shaped laser pulse from 192 NIF beams is converted to thermal x rays in a cylindrical high-Z enclosure referred to as a hohlraum. The x-ray radiation uniformly ablates the surface of a low-Z (CH) spherical ablator shell (r = 1.1 mm), which surrounds a spherical cryogenic layer of solid DT fuel (70 μm thickness, ρ = 0.255 g/cm^3) and central low-density (0.3 mg/cm^3) DT gas fill. The hohlraum x-ray drive launches a series of four shocks to spherically compress the ablator shell and fuel, thereby creating the high density and temperature plasma conditions required to initiate DT fusion reactions in the hot, central fuel core.

To experimentally diagnose and adjust the strength and timing of the shocks, a modified hohlraum geometry (known as the "keyhole" target) is used. A gold diagnostic cone is added, penetrating both the hohlraum and capsule walls, to allow for the direct measurement of shock propagation in the capsule interior. Following the technique first described in [2], the capsule and Au cone are filled with liquid deuterium (D2) at ρ = 0.170 g/cm^3 (replacing the DT ice and gas of an ignition capsule), and the VISAR (Velocity Interferometer System for Any Reflector) diagnostic [3, 4] is used to optically measure the velocity vs. time of the highly reflective leading shock front [5]. Initial experiments demonstrating the shock measurement technique and its application to directly driven implosions on the OMEGA Laser Facility are reported in [6, 7], and results for indirectly-driven implosions on NIF and initial tuning results for NIF ignition pulses are given in [8, 9].

The use of liquid D2 in the tuning targets presents two surrogacy issues: 1.) a material surrogacy (single species D2 vs. two-species DT) and 2.) a geometric surrogacy (the presence or absence of an additional ice / gas interface in the ignition target geometry). Reference [10] presented the initial data assessing these surrogacy assumptions for the first three shocks. Here, a more extensive discussion of

the modified analysis procedures is given together with an extension of the experimental data to include the 4th shock.

To quantify differences in shock strengths between liquid D2 tuning targets and layered DT ice ignition targets, the keyhole target was modified to allow for the growth of DT ice layers. Figure 1(a) shows an x-ray radiograph taken through the LEH of a "thick" DT ice layer grown on NIF (shot N121101). The tip of the Au cone and the inner surface of the Si-doped CH ablator are clearly seen. The gap between these two surfaces was 400 μm. The interface between the DT ice and the equilibrium DT vapor is visualized by x-ray refraction. The uniformity of the layer thickness is shown in Figure 1(b), where the image of Figure 1(a) is "un-folded" to visualize the ice layer thickness relative to the ablator inner surface. The nominal thickness goal of this layer was 300 μm, but considerable variation of the thickness is seen.

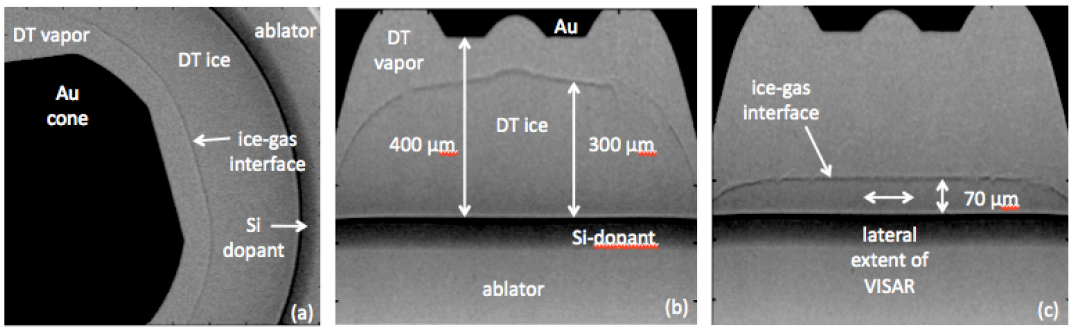

Figure 1. (a) X-ray radiograph of the capsule interior (shot N121101) showing the tip of the Au diagnostic cone, the Si-doped CH ablator, and the contour of a 300 μm thick DT ice layer. (b) Un-wrapped view of the DT ice layer of (a) showing ice thickness variation relative to the ablator inner surface. (c) Un-wrapped view of a 70 μm thick DT ice layer (shot N121108) showing reduced ice thickness variation.

To study the effect of multiple shock release and recompression events from the DT ice to gas, layers of thickness corresponding to those used in ignition targets (nominal value 70 μm [11]) were grown as well. Figure 1(c) shows an example of such a layer (N121108). The thickness uniformity is considerably improved. This is important, as successive shocks will transit the full extent of this layer. The lateral extent of the VISAR measurements at the ablator inner surface is ~350 μm, and the uniformity of the layer thickness over this field-of-view was measured to be better than 1 μm.

2. Geometric surrogacy between continuous liquid D2 and DT ice layer

To explore the geometric surrogacy issue, we now look at the results from thin DT ice layers. Figure 2 shows a comparison of streaked VISAR interferometer data for (a) N121112 (liquid D2) and (b) N121108 (70 μm DT ice layer). Time runs from left to right, and lateral (bottom-to-top) motion of the interference fringes is directly proportional to the shock velocity with fringe motion upward indicating an accelerating shock. Fringe motion is due to reflections from the leading shock front in the fuel (D2 or DT), and discontinuities in the fringe positions indicate the arrival time of shocks. The first of these, labeled "1" and seen at ~13.5 ns, is the time at which the 1st shock breaks out of the CH ablator into the fuel. Subsequent discontinuities indicate the time at which the increasingly stronger 2nd, 3rd, and 4th shocks overtake or merge with preceding shocks.

In Figure 2(a), all 4 shocks are seen, with the arrival time of shocks 2, 3 and 4 close to that desired for optimal ignition tuning. Figure 2(b) shows several new features. The VISAR interferometer signal abruptly ceases at t ≈ 17.5 ns, as the 1st shock passes through the DT ice-gas interface. The resulting rarefaction reflected from this interface generates pressure gradients in the expanding DT ice. As will be quantified later, the reduced pressure in the expanding ice drops below that required for reflectivity of the VISAR laser (λ = 660 nm) [5]. As the 2nd and 3rd shocks traverse this decompressing ice region, they briefly recompress it to the pressure level required for VISAR

reflection. This is seen in Figure 2(b) at t ≈ 18.1 and 19.2 ns as transient returns of VISAR reflectivity. The weaker signal from 19.2 to 20.5 ns is thermal emission from the stronger 3rd shock; here the VISAR is functioning as a Streaked Optical Pyrometer (SOP) [12, 13], recording thermal emission within the band-pass of the VISAR optical system.

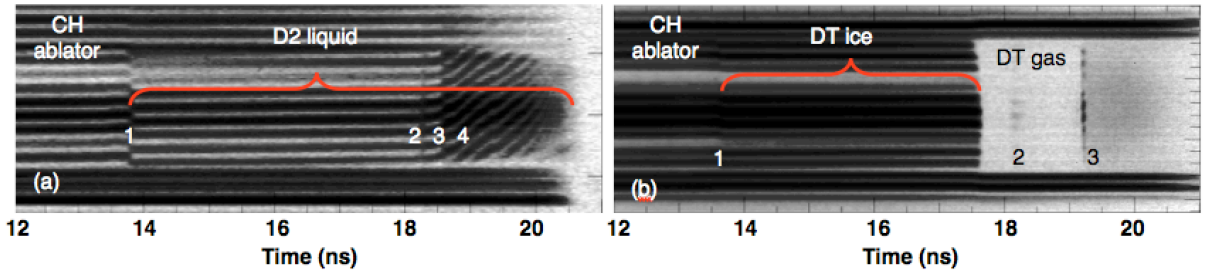

Figure 2. (a) VISAR streaked interferometer images for (a) a standard liquid D2-filled keyhole tuning target and (b) a 70 μm thick DT ice layer. Shock mergers 2 and 3 in (b) occur in the expanding DT gas region.

To analyze the data beyond the time of shock breakout, we use the reported VISAR reflectivity measurements of Celliers [5], where it was shown that VISAR reflectivity in liquid D2 exhibits a threshold response in both electron density ($Ne > Ne_{crit}$) and pressure ($P > 0.5$ Mbar). A metric for VISAR reflectivity from the simulations is proposed as the pressure at critical density. Figure 3 shows contour plots from a 1-D HYDRA [14] simulation to illustrate this. Figure 3(a) is a contour plot of pressure as a function of Lagrangian radius and time. The trajectories of the 4 shocks are superposed on this contour plot. One can clearly see a repeating sequence of shock compression and release events at the inner edge of the DT ice layer with a series of rarefaction waves propagating from the ice/gas interface upward toward the ablator. Figure 3(b) shows the corresponding contour plot of electron number density. The critical density for VISAR absorption or reflectivity is $Ne_{crit} = 2.6e21$ / cm^3. In Figure 3(b), the VISAR critical density is located very near the inner edge of the DT ice layer.

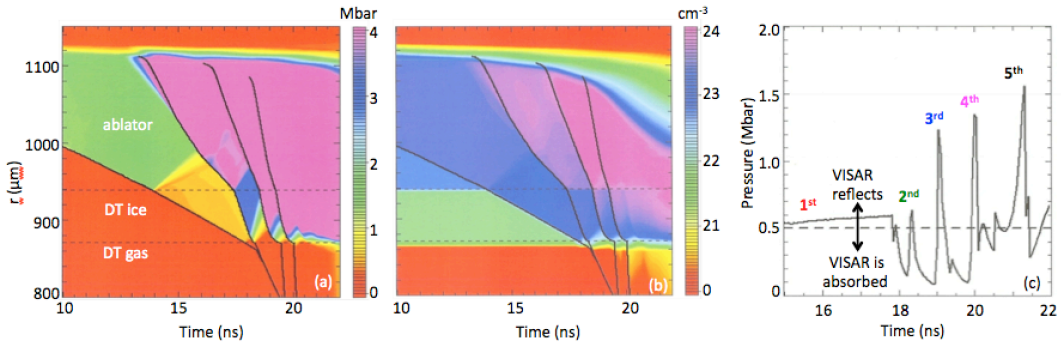

Figure 3. (a) Simulated contours of (a) pressure and (b) electron density plotted as radius vs. time for N130517. (c) Simulated pressure at critical density showing predicted time history of VISAR reflection and absorption.

The physical picture of the VISAR features labeled 2 and 3 in Figure 2(b) is now becoming clearer. These are not the locations of sequential shock mergers, but rather the time at which successive shocks recompress the releasing DT ice material to a pressure above the 0.5 Mbar threshold for VISAR reflectivity. Figure 3(c) plots this metric, the pressure at critical density, from the contour plots of Figures 3(a, b). For the transit of the first shock, this metric shows a continuously increasing pressure of 0.5-0.6 Mbar due to the slightly accelerating 1st shock as it transits the ice layer. Upon shock breakout near 17.7 ns, the pressure abruptly drops as a rarefaction fan is reflected back into the ice layer. At ~18.2 ns, the 2nd shock recompresses this expanding DT and briefly brings the pressure above the 0.5 Mbar threshold for reflectivity. The cycle then repeats, and the same process happens

for the recompression caused by the 2nd, 3rd and 4th shocks. As Figures 3(a-c) show, a 5th shock is also predicted to occur.

Figure 4 applies this new VISAR analysis method to two DT layered keyhole shots to compare the transient reflection features observed after 1st shock breakout with predictions from simulation. Figure 4(a) shows a comparison for shot N121108 (previously discussed in Figure 2(b)). The VISAR streaked interferometer data is shown together with a lineout of the intensity taken through the vertical center of the data. The intensity is high for the first shock as it transits the DT ice, and then drops to a rather low value upon breakout. The two recompression features are seen in the lineout as transient increases in signal intensity. The simulated pressure at critical density is shown on the right-hand side of the Figure. The timing of 1st shock breakout, and 2nd and 3rd shock recompression is in excellent agreement with the data.

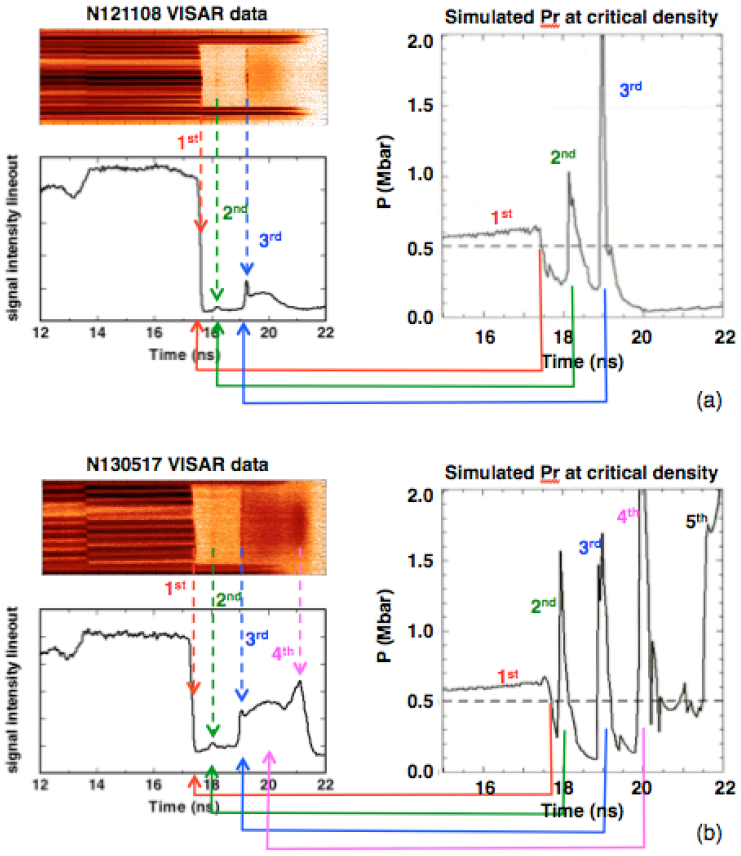

Figure 4. Comparison of measured vs. simulated shock timing for (a) a 3-shock and (b) a 4-shock system.

Figure 4(b) shows a second example of a similar 70 μm DT layer (N130517), but now with the 4th laser pulse included. The data now shows a 4th shock feature beginning at ~20.6 and peaking at 21 ns, whereas no such feature was observed in the VISAR data of Figure 4(a). The timing of 1st shock breakout and 2nd and 3rd shock recompressions is again in excellent agreement with simulation. The experimentally observed 4th shock feature, by contrast, is observed to be 600 ps later than in simulation.

3. Effect of electron preheat on 4th shock timing

There are several possible explanations for the observed discrepancy between simulated and observed 4th shock timing. Any mechanism that causes an additional expansion of the ice layer, for example, would delay the appearance of the 4th shock at the observed critical density for VISAR reflectivity.

Possible mechanisms for such an effect include the DT equation of state (EOS) release behavior, mix at the DT ice/gas interface, x-ray preheat, or supra-thermal (or hot) electron preheat. Since the data and simulations seem to agree for the first three shocks, we need a mechanism that is specific to the timing of the 4th shock. Both EOS release and mix at the ice/gas interface will begin at first shock breakout, so these seem less likely. The current simulations routinely include M-band preheat, which is calibrated by Dante measurements [15], so that leaves hot electron preheat as perhaps the most likely mechanism.

Figure 5 shows the Filter-Fluorescer Experiment (FFLEX) [19] measurements for shot N130517 (DT layer of Figure 4(b)), which are used to infer the hot-electron preheat in NIF hohlraums. FFLEX on NIF consists of 10 time-resolved channels that measure hard x-ray Bremsstrahlung emission over a wide energy range. The FFLEX data are well fit with a two temperature (T1, T2) Maxwellian distribution of supra-thermal electrons. Figure 5(a) shows the preheat power, defined as the power (GW) in the Maxwellian tail for electron energies > 170 keV. As discussed in [11], hot electrons in this energy range can penetrate the ablator and directly heat the DT fuel. Even though there is considerably more preheat energy in the higher temperature (T2) component, it occurs too late to have a significant effect on the 4th shock timing that is observed by VISAR. Inclusion of the T2 component in the simulations has little effect on the observed time of the 4th shock of Figure 4(b).

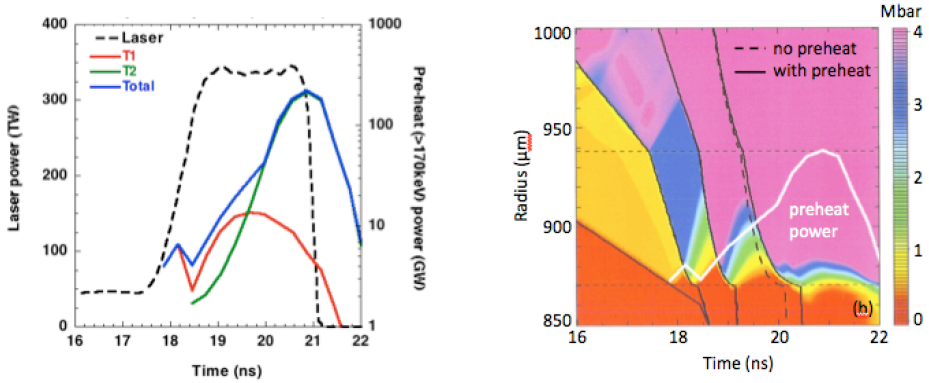

Figure 5. (a) Comparison of measured laser power history for N130517 (black dashed) vs. electron preheat (>170 keV) power. (b) Simulated pressure contours (radius vs. time) with shock trajectories super-posed. Solid black line shows shock trajectories with preheat. Dashed line shows shock trajectories without preheat. White curve is the total (T1 + T2) electron preheat power history.

Inclusion of the lower-temperature (T1) component, however, does have an effect. The supra-thermal electron preheat (both T1 and T2) is included in the HYDRA simulations using the non-local electron transport option, which is an extension of the method of [17]. Figure 5(b) shows the effect of this added preheat on the shock trajectories. The solid (dashed) black lines show the simulated shock trajectories with (without) preheat. The preheat power history is over-plotted with the white curve. The first three shocks are unchanged, but the 4th shock is delayed by approximately 300 ps, which is about half the discrepancy between measurement and simulation observed in Figure 4(b).

Figure 6(a) plots the pressure at critical density from three simulations: one with no electron preheat (black), one with electron preheat from FFLEX measurements (red), and one with twice the FFLEX measured power (blue). The predicted timing of the first three shocks is unchanged, but the timing of the 4th shock is delayed by 300 and 600 ps for the 1X and 2X preheat cases, respectively. This suggests that we need a slightly higher level of electron preheat than that measured by FFLEX to explain the VISAR observations. This could result, for example, from an anisotropic distribution of the electron flux. Note also in Figure 6 that the originally predicted 5th shock feature (black) at ~21.3 ns is completely absent in the simulations with preheat. This agrees with the observations of Figure 4(b), which show only one additional shock feature beyond the 3rd shock, not two.

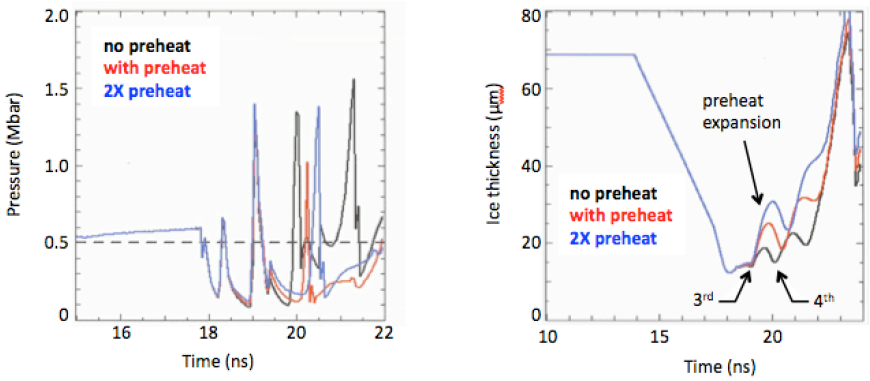

Figure 6. (a) Comparison of simulated pressure at critical density with no electron preheat (black) and with 1X and 2X electron preheat (red and blue, respectively). (b) Temporal evolution of the simulated thickness of the DT ice layer with no electron preheat (black) vs. with 1X and 2X electron preheat (red and blue, respectively).

The delay of the 4th shock timing shown in Figure 6(a) can be further understood by looking at the preheat expansion of the DT ice layer as shown in Figure 6(b). The DT ice layer was originally 68 μm thick. The first three shocks compress the layer by nearly a factor of 6 to ~ 12 μm. With electron preheat added, the layer expands by an additional 7-14 μm during the decompression that occurs between the 3rd and 4th shocks. The 4th shock then re-compresses and exits the ice layer at 20.1 ns (no preheat, black) vs. 20.4 and 20.7 ns (with 1X or 2X preheat), respectively. This preheat induced expansion of the ice layer at 4th shock breakout is a significant fraction (~50%) of the original 3-shock compressed layer thickness and continues to affect the implosion beyond the timing of the 4th shock. Further details and discussion of the implications of this preheat induced expansion on the fuel shell areal density (ρR) and the pressure and density in the hot-spot center are given in [18].

5. Acknowledgements

This work was performed under the auspices of the U.S. Department of Energy by Lawrence Livermore National Laboratory under Contract DE-AC52-07NA27344.

6. References

[1] Lindl J D *et al* 2004 *Phys. Plasmas* **11** 339
[2] Munro D H *et al* 2001 *Phys. Plasmas* **8** 2245
[3] Barker L M and Hollenbach R E 1972 *J. Appl. Phys.* **43** 4669
[4] Celliers P M *et al* 2004 *Rev. Sci. Instrum.* **75** 4916
[5] Celliers P M *et al* 2000 *Phys. Rev. Lett.* **84** (24) 5564
[6] Boehly T R *et al* 2009 *Phys. Plasmas* **16** 056302
[7] Boehly T R *et al* 2011 *Phys. Rev. Lett.* **106** 195005
[8] Robey H F *et al* 2012 *Phys. Plasmas* **19** 042706
[9] Robey H F *et al* 2012 *Phys. Rev. Lett.* **108** 215004
[10] Robey H F *et al* 2013 *Phys. Rev. Lett.* **111** 065003
[11] Haan S W *et al* 2011 *Phys. Plasmas* **18** 051001
[12] Trainor R J *et al* 1979 *Phys. Rev. Lett.* **42** 1154
[13] Miller J E *et al* 2007 *Rev. Sci. Instrum.* **78** 034903
[14] Marinak M M *et al* 2001 *Phys. Plasmas* **8** 2275
[15] Dewald E L *et al* 2004 *Rev. Sci. Instrum.* **75** 3759
[16] Dewald E L *et al* 2010 *Rev. Sci. Instrum.* **81** 10D938
[17] Schurtz G P, Nicolai P D, and Busquet M 2000 *Phys. Plasmas* **7** 4238
[18] Robey H F *et al* 2013 submitted to *Phys. Plasmas*